JOURNAL OF VIROLOGY, Nov. 1998, p. 8578–8585 Vol. 72, No. 11
0022-538X/98/$04.00+0
Copyright © 1998, American Society for Microbiology. All Rights Reserved.

Intracellular Localization of Poliovirus Plus- and Minus-Strand RNA Visualized by Strand-Specific Fluorescent In Situ Hybridization

ROGER BOLTEN,[1]† DENISE EGGER,[1] RAINER GOSERT,[1] GABRIELA SCHAUB,[1] LUKAS LANDMANN,[2] AND KURT BIENZ[1]*

Institute for Medical Microbiology[1] and Department of Anatomy,[2] University of Basel, Basel, Switzerland

Received 28 April 1998/Accepted 21 July 1998

The time courses of poliovirus plus- and minus-strand RNA synthesis in infected HEp-2 cells were monitored separately, using a quantitative RNase assay. In parallel, viral RNA and proteins were located in situ by confocal microscopy within cells fixed by a protocol determined to retain their native size and shape. Plus- and minus-strand RNAs were visualized by fluorescent in situ hybridization (FISH) with strand-specific riboprobes. The probes were labelled with different fluorochromes to allow for the simultaneous detection of plus- and minus-strand RNA. The FISH experiments showed minus-strand RNA to be present in distinct, regularly sized, round structures throughout the viral replication cycle. Plus-strand RNA was found in the same structures and also in smaller clusters of vesicles. Association of viral RNA with membranes was demonstrated by combining FISH with immunofluorescence (IF) detection of the viral 2B- and 2C-containing P2 proteins, which are known to be markers for virus-induced membranes. At early times postinfection, the virus-induced membranous structures were distributed through most of the cytoplasm, whereas around peak RNA synthesis, both RNA-associated membranous structures migrated to the center of the cell. During this process, the plus- and minus-strand-containing larger structures stayed as recognizable entities, whereas the plus-strand-containing granules coalesced into a juxtanuclear area of membranous vesicles. An involvement of Golgi-derived membranes in the formation of virus-induced vesicles and RNA synthesis early in infection was investigated by IF with 2C- and Golgi-specific antibodies.

In a poliovirus (PV)-infected cell, the first virus-specific synthesis is the translation of input plus-strand viral RNA into a polyprotein which is co- and posttranslationally cleaved into functional proteins. While several of these proteins are known to be involved in the replication of the viral RNA, RNA synthesis per se is effected by the viral polymerase $3D^{pol}$ (5, 22, 45). This enzyme first copies input plus-strand RNA into minus-strand RNA, which, in turn, serves as a template for the synthesis of progeny plus strands in the multistranded replicative intermediate (RI) (23).

Data from in vitro experiments indicate that minus-strand RNA synthesis can proceed without cellular structural prerequisites (30, 49). However, membranes may be involved in the initiation step of minus-strand synthesis by presenting membrane-bound 3AB as a precursor of VPg, which is thought to be involved in priming minus-strand synthesis (25, 35).

In contrast, plus-strand RNA synthesis shows distinct structural requirements. In vivo, plus-strand synthesis is associated with specific cellular membranous structures (9, 12, 15) and takes place in a replication complex on the surface of cytoplasmic vesicles induced by the viral protein 2BC (2, 13, 17). In vitro transcription systems, derived from infected cells (11, 14, 21, 41), comprise the replication complex in a rosette-like arrangement of several vesicles surrounding the actual RNA replicating structure (11, 14). Analysis of such systems showed that the membranes of the vesicles are necessary for initiation of RNA synthesis but dispensable for elongation of RNA (20). However, the exact role of membranes in cell-free systems, derived from uninfected cells and replicating PV de novo, is not yet established (6, 7, 27, 28, 43).

The role of membranes in viral plus-strand RNA synthesis in infected cells or subcellular fractions, as summarized above, was investigated mostly at late times postinfection (p.i.), i.e., when vesicle formation and RNA synthesis were at their peaks. Only little information on membrane association of viral plus-strand RNA synthesis at early times of infection is available. Likewise, the location of viral minus-strand RNA synthesis is largely unknown. Therefore, in the present investigation we determined the intracellular location of minus-strand RNA in comparison with that of plus-strand RNA over time. This would allow for a better understanding of the interdependence of and possible differences in the mechanisms governing plus- and minus-strand RNA synthesis.

To address these questions, the locations of plus- and minus-strand RNAs were determined by fluorescent in situ hybridization (FISH) with confocal microscopy. The use of plus- or minus-strand-specific riboprobes, each labelled with a different fluorochrome, allowed for the simultaneous detection of plus- and minus-strand RNA. Association of viral RNA with membranes was determined by combining FISH and immunofluorescence (IF) detection of the viral 2B- and 2C-containing P2 proteins, which served as a marker for virus-induced membranes (9, 10, 39).

Minus-strand RNA could be detected in distinct, regularly sized, round membranous structures also containing plus-strand RNA and remaining constant in amount and size over the entire viral growth cycle. Plus-strand RNA was additionally found at early times, i.e., before peak RNA synthesis, in small clusters of vesicles, as judged from its colocalization with P2 proteins. Around peak synthesis, all RNA-associated membra-

* Corresponding author. Mailing address: Institute for Medical Microbiology, University of Basel, Petersplatz 10, CH-4003 Basel, Switzerland. Phone: 41 61 267 3290. Fax: 41 61 267 3298. E-mail: Bienz @ubaclu.unibas.ch.

† Present address: Drossapharm, Arlesheim, Switzerland.

nous structures migrate to the center of the cell to form a characteristic juxtanuclear area of vesicles, with the distinct plus- and minus-strand-containing compartments still being clearly delineated. Interestingly, the two compartments could be distinguished only by FISH, according to their RNA content, and not on an ultrastructural level.

MATERIALS AND METHODS

Cells and virus. HEp-2 cell suspension cultures were infected with PV type 1 Mahoney at a multiplicity of infection of 30 PFU. The virus was allowed to adsorb at 4°C for 30 min in serum-free medium (Joklik minimal essential medium) (Seromed, Berlin, Germany). The cells were then washed once in cold serum-free medium and incubated at 36°C in medium containing 10% calf serum.

Isolation of RNA from infected cells. At various times p.i., 10^6 to 10^7 cells were washed twice in cold serum-free medium. The RNA was isolated from the cell pellet by using Trizol reagent (Gibco BRL, Gaithersburg, Md.) according to the instructions of the manufacturer.

In vitro transcription of RNA for RNase protection assays (RPAs). All PV-specific RNAs were derived from plasmid pT7PV, containing the full-length genome of PV type 1 Mahoney (16). The [α-^{35}S]UTP (Amersham International, Little Chalfont, United Kingdom)-labelled plus-polarity riboprobe consisting of nucleotides (nt) 1 to 220 (riboprobe nt 1–220) was transcribed with T7 RNA polymerase (Boehringer, Mannheim, Germany) from a gel-purified *Bam*HI fragment of pT7PV. The ^{35}S-labelled minus-polarity riboprobe nt 6065–6276 (numbering as for the positive-sense sequence) was prepared by transcription with T7 polymerase of PCR-amplified cDNA nt 6012–6276-T7, trimmed with *Hin*dIII and gel purified. Unlabelled RNAs nt 1–595 (plus polarity), nt 1–460, and nt 6012–6736 (both plus and minus polarity) were transcribed from corresponding cDNA fragments which were PCR amplified from *Eco*RI-linearized pT7PV DNA by using appropriate primers of 18 to 20 nt in length preceded by SP6 or T7 promoter sequences (40, 50).

RPA for detection of plus-strand RNA. Ten picomoles of ^{35}S-labelled riboprobe nt 6065–6276 of minus polarity was added to RNA extracted from infected cells. Hybridization was done in 20 μl of 80% deionized formamide–100 mM sodium citrate (pH 6.4)–300 mM sodium acetate (pH 6.4)–1 mM EDTA at 48°C overnight. RNase digestion was done at 37°C by adding 200 μl of RNase buffer (10 mM Tris HCl [pH 7.5], 1 mM EDTA, 200 mM NaCl, 100 mM LiCl) containing 0.35 U of RNase A per ml and 13.5 U of RNase T_1 per ml (Boehringer). After proteinase K digestion (final concentration, 0.13 mg/ml; Boehringer) and ethanol precipitation, RNA corresponding to 1.25×10^5 (late times p.i.) to 1×10^7 (early times p.i.) cells was separated on a 2.5% NuSieve (FMC, Rockland, Maine) denaturing agarose gel, blotted as described previously (20), visualized by autoradiography, and quantitated on a CDS200 densitometer (Beckman, Palo Alto, Calif.).

Two-cycle RPA for detection of minus-strand RNA. Before the first hybridization step of the two-cycle RPA (31), an excess of 1 μg of unlabelled RNA nt 1–595 of plus polarity was added to the RNA from 5×10^6 to 1×10^7 Trizol-extracted cells to ensure full protection of all minus strands. Hybridization was done in 40 μl of 4 M guanidine thiocyanate in 25 mM sodium citrate at 37°C overnight. RNase digestion (to eliminate excess single-stranded plus-strand RNA) was done in 400 μl of buffer (50 mM Tris HCl [pH 7.5], 10 mM EDTA, 400 mM NaCl) containing 5.7 U of RNase A per ml and 0.3 U of RNase T_1 per ml (Boehringer) at 37°C for 30 min. After proteinase K digestion and phenol extraction, the samples were put through the same RPA as described for plus-strand detection, using 10 pmol of the ^{35}S-labelled riboprobe nt 1–220 of plus polarity.

Standards for quantitative RNA determinations. Dilution series of known amounts of unlabelled standard RNA hybrids were subjected to the same RPA as used for RNA from infected cells. As a standard for the quantitation of plus-polarity viral RNA, double-stranded RNA of nt 6012 to 6736 and a ^{35}S-labelled probe (nt 6056 to 6276) of minus polarity were used. For minus-strand viral RNA, double-stranded RNA of nt 1 to 460 and a ^{35}S-labelled probe (nt 1 to 220) of plus polarity were used.

Preparation of cells for confocal microscopy. After infection with PV type 1 Mahoney, 1.5×10^6 HEp-2 cells were dispersed on poly-L-lysine-coated coverslips at various times p.i. After adhesion to the coverslips for 4 min, cells were fixed for 10 min at room temperature by gentle immersion in 4% paraformaldehyde in PBS and permeabilized with 0.2 to 0.3% Triton X-100 in 4% paraformaldehyde for 10 min. After a phosphate-buffered saline (PBS) wash, aldehydes were quenched in 0.5 M ammonium chloride in PBS for 7 min. The coverslips were washed twice in PBS and processed for FISH and IF.

FISH. For plus-strand RNA detection, two riboprobes of minus polarity were prepared from appropriate DNA fragments that had the T7 promoter sequence added by PCR. The probe nt 1–7441 was labelled with fluorescein isothiocyanate (FITC)-UTP (Boehringer) during in vitro transcription, and the probe nt 6875–7441, used in double-FISH experiments, was labelled with Texas red-UTP (Molecular Probes, Eugene, Oreg.). Unincorporated nucleoside triphosphates were removed with a Micro Bio-Spin 6 column (Bio-Rad, Hercules, Calif.). To ensure good penetration of the probes into the fixed and permeabilized cells, the probes were subjected to alkaline hydrolysis (18) to generate fragments of approximately 100 nt in length. Occasionally, a second column (Bio-Spin 30) was used to remove oligonucleotides of less than 20 nt in length. The riboprobe was dissolved in hybridization buffer (50% formamide, 10 mM Tris-HCl [pH 7.4], 600 mM NaCl, 10% dextran sulfate, 10 mM dithiothreitol, 0.05% bovine serum albumin, 0.1% sodium dodecyl sulfate, 200 μg of salmon sperm DNA per μl, 100 μg of yeast tRNA per μl) and hybridized to the cells at 40°C overnight. After four washes in 0.1× SSC (1× SSC is 0.15 M NaCl plus 0.015 M sodium citrate) for 10 min, the slides were mounted with 33.3% (vol/vol) glycerol containing 16.6% (wt/vol) Mowiol (Hoechst, Frankfurt, Germany) and 2.5% (wt/vol) 1,4-diazabicyclo[2.2.2]octane (DABCO) (Sigma, Buchs, Switzerland).

For minus-strand RNA detection, an FITC-labelled and hydrolyzed riboprobe nt 1–6867 of plus polarity was used. The minus-strand-specific probe contained approximately 10 times more of the PV sequence than the plus-strand-specific probe in order to compensate in signal intensity for the small amount of minus-strand RNA present in the infected cells. Prior to hybridization with the minus-strand-specific probe, cells attached to the coverslips were denatured in 95% formamide in 0.1× SSC at 65°C for 10 min. After being chilled and washed in 0.1× SSC, the cells on the coverslips were hybridized with the minus-strand-detecting probe as described above for plus-strand detection.

Controls included identically treated mock-infected cells and an unrelated RNA probe (dengue virus type 2 nt 134 to 252, of minus polarity) prepared and used as described for the PV-specific probes.

IF. The preparation and specificities of monoclonal antibodies (MAb) directed against proteins 2C and 2B were described earlier (20, 33). The MAb were used for an indirect IF assay with goat anti-mouse immunoglobulin G (IgG) coupled to Texas red (Molecular Probes). For colocalization studies of Golgi complexes and protein 2C, an anti-Golgi 58-kDa protein mouse MAb (Sigma) and a rabbit anti-2C polyclonal Ab (17) were used. IF detection was done with goat anti-mouse IgG coupled to Texas red and goat anti-rabbit IgG coupled to FITC (Sigma). Images were recorded on a Leica TCS4D confocal microscope equipped with appropriate filter sets. The photomultiplier settings were adjusted so that no Texas red signal could be detected in the FITC channel and vice versa. Raw images were corrected for contrast, intensity, and background fluorescence by using Adobe Photoshop software.

Electron microscopy (EM). Cells were fixed in glutaraldehyde and OsO4 and embedded in Poly/Bed 812 (Polysciences, Warrington, Pa.) by standard protocols (8).

RESULTS

Kinetics of plus- and minus-strand RNA synthesis. To correlate the results of the FISH experiments reported below with those of the time course experiments, particularly the peaks of plus- and minus-strand viral RNA synthesis, we monitored the replication of PV plus- and minus-strand RNAs separately by RPA. For plus-strand detection, a ^{35}S-labelled probe of minus polarity spanning nt 6065 to 6276 (numbering is as for the positive-sense RNA of PV type 1 Mahoney) was used, and for minus-strand detection, a two-cycle RPA was performed as described previously (31) with a ^{35}S-labelled probe of plus polarity (nt 1 to 220).

Figure 1 shows, in agreement with earlier findings (3, 31, 32), that the ratio of the amount of plus-strand RNA to that of minus-strand RNA increases up to 100-fold during the replication cycle. As inferred from results with standard hybrids processed in parallel, the total yield of viral RNA was approximately 10^4 minus strands and 10^6 plus strands per cell at 4.5 h p.i. The time courses of plus- and minus-strand syntheses proved to be very similar (Fig. 1b): both syntheses show peak activity at between 3 and 3.5 h p.i., with 50% of both plus and minus strands already synthesized at that time. The amount of minus-strand RNA synthesized at each time point was fairly constant, in the range of 1 to 2% of the amount of plus strands synthesized at the same time.

FISH of plus- and minus-strand viral RNA. To visualize plus- and minus-strand PV RNAs separately, we performed FISH experiments with nonoverlapping plus- and minus-strand-specific RNA probes. The probes, labelled with different fluorochromes during in vitro transcription, were used either separately or, mixed together, simultaneously on the same slide. Plus-strand RNA was detectable without pretreatment of the slides (8), whereas detection of minus-strand RNA was

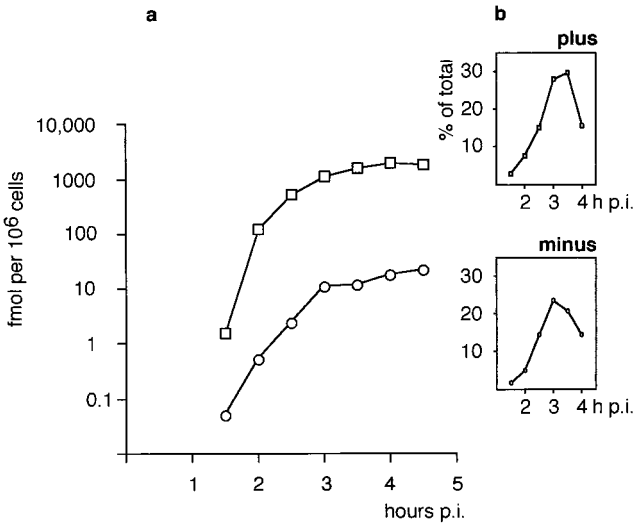

FIG. 1. Kinetics of plus- and minus-strand RNA synthesis in PV-infected HEp-2 cells as determined by RPA. (a) Time p.i. versus amounts (logarithmic scale) of plus (□)- and minus (○)-strand RNA synthesized. (b) Peak synthesis of plus- and minus-strand RNA is between 3 and 3.5 h p.i.

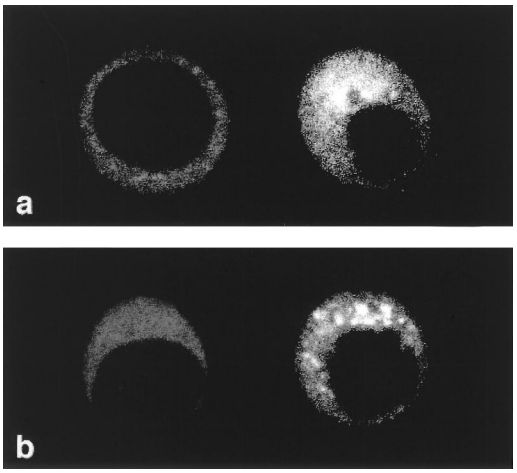

FIG. 2. Evaluation of background staining in FISH with uninfected (left) and PV-infected (right) cells in the same microscopic field with a Texas red-labelled plus-strand-specific probe (a) and an FITC-labelled minus-strand-specific probe (b). For an explanation of structural details, see the legend to Fig. 3.

possible only after thermal denaturation of the specimen at 65°C for 5 to 10 min, similar to earlier findings with in situ hybridization on sections (44).

Because of the small amount of minus-strand RNA present, maximal sensitivity for minus-strand detection was needed. This was achieved by using directly FITC-labelled probes to avoid immunological detection, a step found to reduce the hybridization signal considerably (data not shown). The reduction was found to be due to Ab preparations containing endogenous RNase (data not shown) that digested any probes and targets that were incompletely hybridized. Generally, sensitivity could be enhanced by using RNA fragments of approximately 100 nt, derived from FITC- or Texas red-labelled probes by alkaline hydrolysis. To at least partially compensate for the different amounts of plus- and minus-strand RNAs present in the infected cells, in experiments for simultaneous detection of both polarities the minus-strand-specific probe was chosen to span approximately 10 times more (nt 1 to 6867) of the polio RNA than the plus-strand-specific probe (nt 6875 to 7441).

In order to be able to estimate background fluorescence and to compensate for it during the final digital image processing, we included mock-infected cells in the preparations. It was found that the level of background fluorescence was dependent on the concentration of the fluorescent RNA probe used. Therefore, probes were pretested in dilution series in hybridizations on such mixed preparations. Working concentrations found to be optimal were usually on the order of 30 to 100 ng of RNA per hybridization assay mixture of 15 μl on one slide (data not shown). When such titrated probes were used, neither plus (Fig. 2a)- nor minus (Fig. 2b)-strand-specific FISH induced background fluorescence in mock-infected cells.

Initially, FISH and IF for confocal laser microscopy were done on Cytospin preparations. However, with such preparations we could not rule out artificial localization of the targets. Centrifugation resulted in flattened cells with a perinuclear rim of cytoplasm in which the target molecules seemed to accumulate. Therefore, cells were fixed by a method that avoided mechanical stress (see Materials and Methods) in order to keep the dimensions and proportions of the cells comparable to those in vivo. This was confirmed by measuring cell thickness along the *z* axis by confocal microscopy.

With the FISH protocol employed, we were able to detect plus-strand RNA as early as 1.5 h p.i. As shown in Fig. 3A, panel a, plus-strand RNA (red) is accumulated in small, irregularly sized granules spread out in the cytoplasm. Gradually, the granules increase in number and migrate toward the inner part of the cell, although in most cases a central area is left free. From 3.0 h p.i. on, the granules are found concentrated in a round, juxtanuclear area (Fig. 3A, panel d), which corresponds to an accumulation of virus-induced vesicles involved in RNA synthesis, as described previously (9, 10, 19, 39, 44).

In contrast, minus-strand RNA (green) is associated with fewer and larger structural entities, which are less spread out

FIG. 3. Viral RNA and protein detected in PV-infected HEp-2 cells by fluorescent confocal microscopy. Bar, 5 μm. (A) Simultaneous visualization of viral plus- and minus-strand RNA in the same cell by double-labelling FISH. Plus-strand RNA (panels a and d), detected with a Texas red-labelled riboprobe of minus polarity, is found in several small granules, at first dispersed and later in infection concentrated in a juxtanuclear area. Minus-strand RNA (panels b and e), detected with an FITC-labelled riboprobe of plus polarity, is present in larger, distinct granules. Superimposed plus- and minus-strand detection shows colocalization of both signals in yellow (panels c and f). Panels a to c, 2.5 h p.i.; panels d to f, 3.5 h p.i. (B) Minus-strand RNA, detected with an FITC-labelled riboprobe as for panel A, remains in distinct granules throughout the replication cycle. Panel a, 2.25 h p.i.; panel b, 2.5 h p.i.; panel c, 3.0 h p.i.; panel d, 3.5 h p.i. (C) Simultaneous visualization of viral plus-strand RNA and viral protein 2C by combined FISH and IF. Plus-strand RNA (panels a and d) is detected with an FITC-labelled riboprobe. Protein 2C and 2C-containing precursors (panels b and e) are detected with an anti-2C MAb and Texas red-labelled anti-mouse IgG. Superimposed FISH and IF show that early in infection, plus-strand RNA and 2C are colocalized (yellow in panel c); at later times some dissociation of 2C from RNA is visible (panel f). Panels a to c, 2.0 h p.i.; panels d to f, 3.5 h p.i. (D) IF with a MAb against Golgi protein p58 detected with Texas red-labelled anti-mouse IgG, combined with IF with a polyclonal rabbit anti-2C Ab detected with an FITC-labelled anti-rabbit IgG. Panel a, intact Golgi complexes at 2 h p.i. Panel b, the same cells as in panel a, showing IF with anti-2C Ab superimposed. Little colocalization (yellow) of the two targets is found. Panel c, superimposed pictures of a cell double labelled by IF with anti-p58 and anti-2C Ab at 2.5 h p.i. The Golgi marker and viral protein 2C colocalize partially. Panel d, superimposed pictures as in panels b and c at 3 h p.i. The Golgi marker is distributed in the cytoplasm and is colocalized with protein 2C mainly at the border of the juxtanuclear area of vesicles.

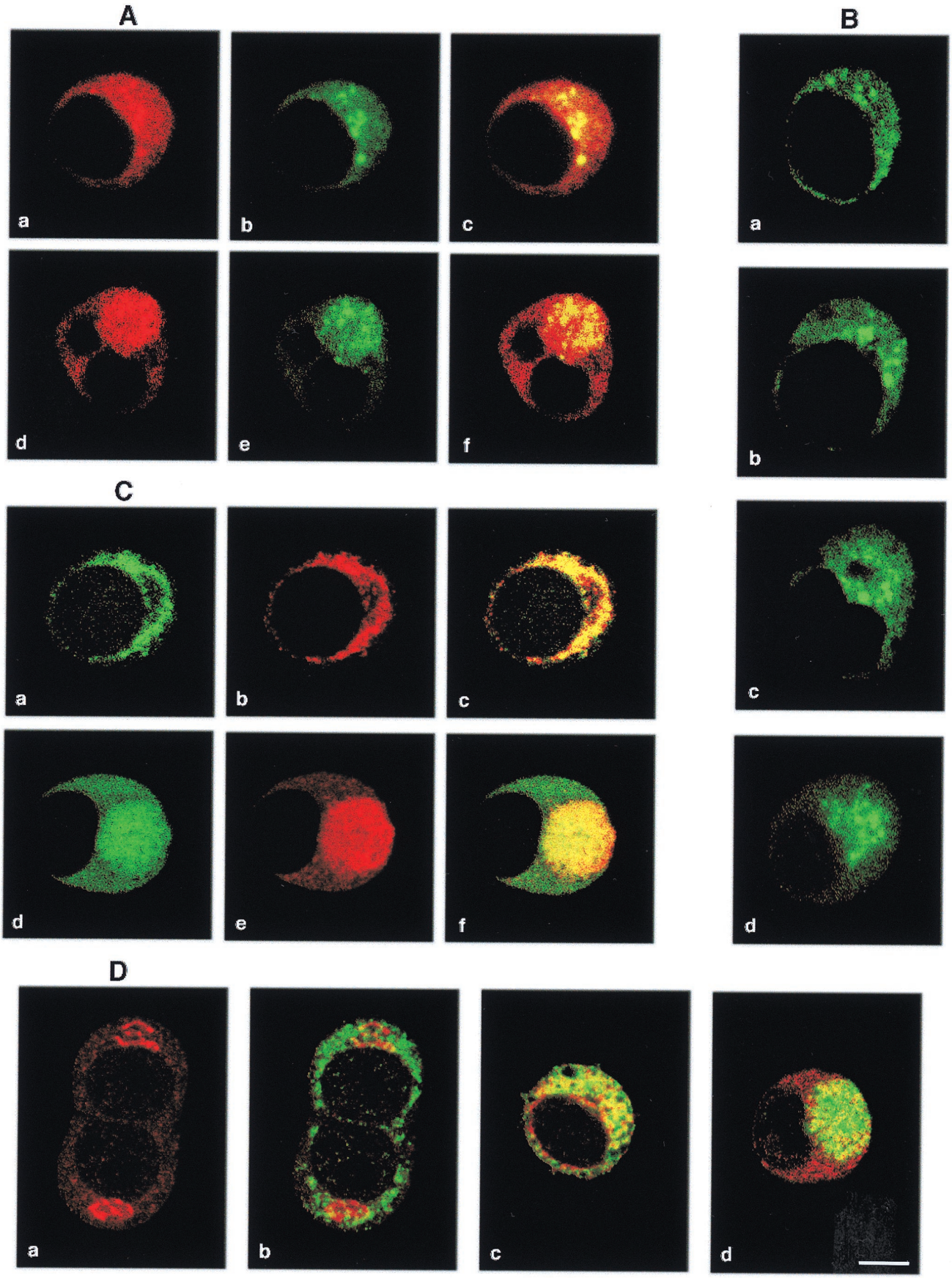
A
a
b
c
d
e
f
B
a
b
c
d
C
a
b
c
d
e
f
D
a
b
c
d

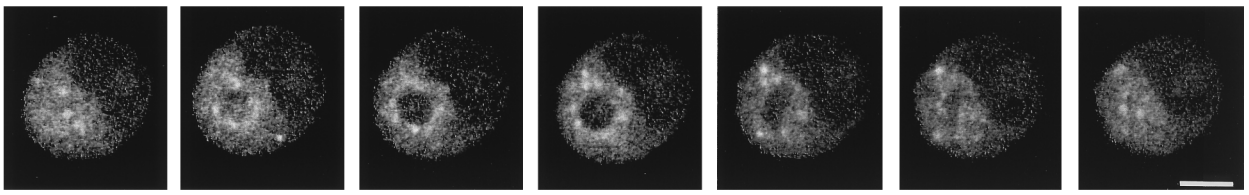

FIG. 4. FISH for minus-strand detection in a series of optical sections, spaced 0.4 μm apart, through an infected cell at 2.75 h p.i. Minus-strand RNA is found in single spherical granules of approximately 0.5 μm in diameter in a symmetrical array around an unlabelled center. Bar, 5 μm.

through the cytoplasm (Fig. 3A, panel b). The number, size, and shape of the minus-strand signals remain rather constant during the replication cycle (Fig. 3A, panel e), and the signals virtually always colocalize with those for plus-strand RNA (Fig. 3A, panels c and f, yellow signal), whereas a substantial amount of plus-strand RNA shows no overlap with minus-strand RNA. The presentation of the plus- and minus-strand FISH signals in separate pictures (Fig. 3A, panels a, b, d, and e) allows a better recognition of the size, shape, and intracellular location of the target molecules, whereas superimposed pictures (Fig. 3A, panels c and f) demonstrate, in yellow, the extent of colocalization of the two targets.

Figure 3B shows the evolution of the minus-strand-containing structures over time. The initially (at 2.25 h p.i.) randomly distributed dots (Fig. 3B, panel a) migrate toward the center of the cytoplasm. However, they do not form a compact juxtanuclear area but stay as individual granules. A central part among the aggregated granules often remains empty (Fig. 3B, panel c).

Figure 4 shows a series of selected optical sections (spacing, 0.4 μm) through an infected cell at 2.75 h p.i. with FISH for minus-strand detection performed. The single minus-strand-RNA-containing granules are spherical, approximately 0.5 μm in diameter, and quite symmetrically grouped around an unlabelled center, thus forming an empty raspberry-like ball.

To test whether the structures seen by FISH correspond to PV-specific vesicular structures, PV-infected cells were processed in parallel for EM and evaluated for membrane alterations. The first detectable vesicles were found in small clusters at 2 h p.i. (Fig. 5). The time course of appearance and intracellular distribution of the clusters suggest that they correspond to the plus-strand-RNA-containing granules observed by FISH (Fig. 3A, panel a). However, no structural entity could be recognized which would correspond per se to the larger plus- and minus-strand-containing bodies (Fig. 3A, panels b and e) observed in the confocal microscope. Thus, we propose that such a structure might be made from a cluster of vesicles.

Combined localization of viral RNA and P2 proteins. The viral P2 proteins 2B, 2C, and 2BC are known to be markers for virus-induced membranes and have been found to be associated with the RI-containing replication complex in the juxtanuclear area of vesicles (9–11, 14). We wanted to know whether the early plus-strand-RNA-containing granules observed with the confocal microscope are composed of 2B- and 2C-containing membranes and thus presumably carry conventional replication complexes. To test this hypothesis, we com-

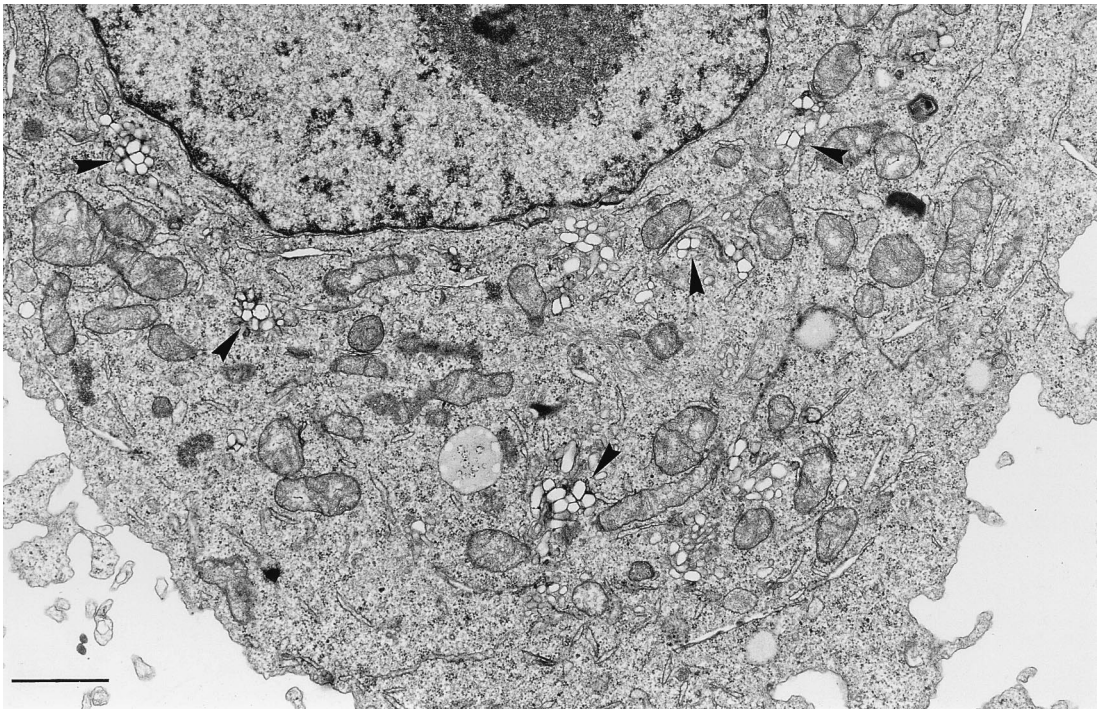

FIG. 5. Electron micrograph of a PV-infected HEp-2 cell at 2 h p.i., showing individual small clusters of virus-induced vesicles (arrowheads). Bar, 1 μm.

bined FISH for plus-strand detection and IF for P2 protein localization with MAb specific for 2C, thus recognizing proteins 2BC and 2C. Figure 3C, panel c, shows an almost-perfect colocalization (yellow) of the P2 signals (Texas red) (Fig. 3C, panel b) with plus-strand RNA (FITC) (Fig. 3C, panel a) at early times p.i. After 3 h p.i., i.e., when a compact juxtanuclear area of vesicles is formed, the protein signal (red) dissociates partially from that of the plus-strand RNA (green) (compare panels d and e in Fig. 3C) and tends to accumulate more toward the border of the juxtanuclear area, leading to a partially nonhomogeneous appearance of this area in superimposed IF-FISH images (Fig. 3C, panel f). Combining FISH and IF analysis with an anti-2B MAb gave virtually the same result (not shown).

To determine whether the larger granules containing plus- and minus-strand RNA (Fig. 3B) are composed of the same species of 2C-carrying vesicles, FISH for minus-strand detection and IF for P2 protein detection were combined. However, this combination did not yield reliable IF results, due to the destruction of the antigenic epitope by the thermal denaturation employed in the FISH protocol for minus-strand detection (not shown). Nevertheless, since minus-strand RNA fully colocalizes with plus-strand RNA (Fig. 3A), minus-strand RNA can also be considered to associate with P2-containing vesicular structures at early times in the infectious cycle. A comparison of the intracellular distributions of P2 proteins, plus-strand RNA, and minus-strand RNA in the juxtanuclear vesicular area after 3 h p.i. (Fig. 3A and C) suggests that both species of viral RNA and the P2 proteins still colocalize and only a small amount of 2BC and 2C segregates from the RNA-associated structures.

Early in infection, the Golgi complex is not the unique origin of the virus-induced vesicles. The onset of viral plus-strand RNA synthesis in peripheral, separated clusters of vesicles led us to investigate whether these early clusters originated from Golgi-derived vesicles, as suspected previously for morphological reasons (13) and as inferred from immunocytochemical studies implicating 2B as a Golgi-targeted viral protein (37). The presence of Golgi components in virus-induced vesicles has also been shown recently by immunoprecipitation, albeit for vesicles late in the infection (39). Since Golgi markers proved to be too delicate as antigens for the FISH conditions, even without thermal denaturation, we compared instead the location of Golgi markers with the location of the vesicle- and replication complex-associated 2C-containing P2 proteins (9, 14, 20, 39). Figure 3D, panel a, shows that at 2 h p.i. Golgi complexes (Texas red) are still intact, and only very few 2C (FITC) and Golgi epitopes colocalize (yellow) (Fig. 3D, panel b). At 2.5 h p.i., the Golgi complex starts to disintegrate, with the corresponding marker becoming distributed throughout the cytoplasm (Fig. 3D, panel c). There is some overlap between the Golgi marker- and the 2C-specific signals. At 3 h p.i. (Fig. 3D, panel d), P2 protein-carrying vesicles become condensed in the juxtanuclear vesicular area, whereas Golgi membranes remain spread out in the cytoplasm. Some colocalization (yellow) of both markers is found, particularly at the border of the juxtanuclear area. These observations argue against an origin of the vesicular clusters from Golgi complexes early in infection but are compatible with a contribution of Golgi membranes or membrane components to virus-induced vesicles in the juxtanuclear area (39).

In conclusion, our IF and FISH findings show that viral plus- and minus-strand RNA is associated with virus-induced vesicles as soon as RNA and vesicles become detectable. They suggest that the population of ultrastructurally similar vesicles consists of higher-order structures which are functionally different in plus- and minus-strand RNA synthesis.

DISCUSSION

In our virus-cell system, plus- and minus-strand viral RNA syntheses peak at the same time, i.e., at 3 to 3.5 h p.i. (Fig. 1). Concomitantly, a rapid and drastic change in the array of virus-induced membrane structures occurs, in that all replication-associated vesicles migrate toward a central area of the cell where they accumulate (Fig. 3A, panels d to f). We attempted to compare the viral RNA locations before and after this breakpoint and particularly to monitor the appearance of viral minus-strand RNA. Detection of viral RNA by RPA as well as localization of plus-strand RNA by FISH with the confocal microscope gave positive results as early as 1.5 h p.i.; minus-strand RNA was detected at 2 h p.i. by FISH. Virus-specific RNA synthesis must occur still earlier, but at present this remains beyond the detection limit.

The earliest morphological changes detectable in a PVirus-infected cell by EM were found at around 1.5 to 2 h p.i. The changes consist of small clusters of vesicles scattered through the cytoplasm. It has been suggested that such early vesicles might be Golgi derived (13) and that the Golgi complex represents an early target for PV replication (37). Therefore, we tested by double IF whether the P2 proteins, indicative of virus-induced vesicles, colocalized to the Golgi. The results obtained indicate that the membranes of the emerging virus-induced vesicular clusters are not, or are only in minute amounts, Golgi derived and thus that viral RNA synthesis employs, at its beginning, few if any Golgi-derived vesicles. However, later in infection and after virus-induced disruption of Golgi complexes, Golgi-derived membranes were found redistributed throughout the cytoplasm (37, 39) and colocalized partially to the virus-induced vesicles (Fig. 3D, panel d). This is compatible with the finding that Golgi marker proteins are present in isolated P2-containing virus-induced vesicles (39). It is not known whether the vesicles bearing Golgi markers originate in toto from the Golgi complex or whether they arise by fusions between Golgi- and endoplasmic reticulum-derived membranes.

The in situ detection of viral minus-strand RNA became feasible only with the use of strand-specific riboprobes directly labelled with the fluorochrome, which obviated any further, e.g., immunological, detection of the hybridized probe. Viral minus-strand RNA was found to be contained in relatively large, round bodies of regular size, which kept the same appearance throughout the replication cycle. Interestingly, no ultrastructural equivalent of the large, minus-strand-RNA-containing dots could be identified. Thus, these dots are defined by RNA and protein contents as determined by confocal microscopy, and they are considered to correspond, on the EM level, to morphologically nondelineated clusters or aggregates of virus-induced vesicles.

Colocalization experiments visualizing plus- and minus-strand RNA in the same cell showed viral RNA to be present in two different structures: the large round bodies, which harbor plus-strand RNA in addition to minus-strand RNA, and small granules which carry plus-strand RNA and lack a recognizable minus-strand-specific signal. From the observation that both structures carry P2 proteins, which are known to be exclusively membrane bound (9, 14, 20, 39), and from a comparison with EM data, we conclude that both structures correspond to aggregates of virus-induced vesicles.

The intracellular dispersed location of both structures changed around peak RNA synthesis, when they migrated cen-

tripetally into a juxtanuclear area. There, the smaller clusters, containing only plus-strands, coalesce, whereas the larger, plus- and minus-strand-RNA-containing dots remain as recognizable entities. The highly ordered redistribution of the individual vesicular clusters is indicative of a distinct and elaborate spatial organization of the RNA synthetic activities within the infected cell.

The presence of two distinct compartments as defined by appearance as well as RNA content suggests that they also differ in certain functions in RNA replication. Previously, we have shown by EM autoradiography that not only the compact juxtanuclear vesiculated area but also clusters of vesicles, as observed early in the infectious cycle, are involved in viral RNA synthesis (9). A comparison of the EM autoradiography and the FISH data suggests that viral plus- and minus-strand RNA synthesis is vesicle associated from the beginning. However, a reevaluation of our high-resolution EM autoradiography data did not allow us to define structures or areas corresponding to the larger, plus- and minus-strand-RNA-containing distinct bodies.

The pattern of the autoradiography signal suggests that the large plus- and minus-strand-containing bodies are not the exclusive structures of plus-strand RNA synthesis in the RI. This is also made likely by the observation that the FISH signal of a probe recognizing the 5′ end of the plus strand does not preferentially label the minus-strand-containing bodies, clearly not more than the 3′ probe used in this paper (not shown). This argues against predominantly nascent plus strands, i.e., RIs, in these bodies. We propose rather that these structures represent the site of viral minus-strand RNA synthesis and that this activity might be followed closely by plus-strand initiation. The resulting newly induced RI might then soon leave this compartment to continue further plus-strand synthesis on the plus-strand-specific vesicular structures (Fig. 3A) (11), where mature plus strands would accumulate (44). Thus, we propose that the plus- and minus-strand-RNA-containing bodies represent the starting points, or germ centers, of viral RNA replication.

The P2 proteins 2B and 2C and their precursor 2BC have all been found to be directly or indirectly involved in viral RNA replication (7, 26, 34, 42, 46–48), although the exact roles of these proteins are only partially understood. Our data show the P2 proteins to be colocalized primarily with all of the plus-strand FISH signals and not preferentially with the plus- and minus-strand-RNA-containing bodies. This indicates an involvement of these proteins in plus-strand synthesis (4), in addition to their proposed role in minus-strand synthesis, as concluded from data obtained with a cell-free translation-transcription system (7). Since the juxtanuclear area of vesicles acquires new vesicles at its periphery, the margination of the P2 proteins in this area at later times is still compatible with a role of 2C in the organization of the plus-strand replication complex (14) and with a role of protein 2BC in the induction of its vesicles (1, 2, 13, 17).

It was found that continuous lipid synthesis, and thus vesicle formation, is necessary for ongoing viral plus-strand RNA synthesis (24). It is tempting to speculate that the large, presumably minus-strand-synthesizing bodies stay at their constant size because membrane synthesis, and thus an increase in the number of vesicles, is not required for minus-strand RNA synthesis.

For many RNA virus families, including picornaviruses, flaviviruses, togaviruses, and a series of picornavirus-like plant viruses, membrane-dependent replication complexes have been described (reviewed in references 36 and 38). The detailed structures of these complexes as well as the exact biochemical contributions of membranes to virus replication are still largely unknown. Despite the functionality of a single vesicle in initiating and sustaining plus-strand RNA synthesis (20), PV-induced vesicles show a high tendency to accumulate into higher-order rosette-like structures (14), presumably thereby increasing the efficiency of plus-strand RNA synthesis. Even though minus-strand synthesis per se might not require membranes (29, 49), sequestration of plus-strand templates for minus-strand synthesis in the large minus-strand-containing bodies described in this paper might still be advantageous in order to avoid competition for plus strands by the translational machinery.

The observation (Fig. 1) (32) that the viral plus- and minus-strand RNA syntheses run in parallel at a constant ratio seems to indicate that the syntheses might be quantitatively interdependent, e.g., by mutually supplying the respective RNA templates. At present, the mechanism controlling this linkage is elusive. Generally, very little is known about regulation of PV replication in the sense of feedback mechanisms governing the quantitative and qualitative synthesis of viral molecules. Even the hallmark of picornavirus replication, i.e., the proteolytic cleavage of the polyprotein, implies that the entire set of gene products is present during the whole viral replication cycle and consequently that there are no early and late functions. Likewise, our findings that plus- and minus-strand RNAs are found in distinct compartments during the entire viral replication cycle could mean that PV replication depends primarily on mechanisms where a (most likely structural) constraint(s) regulates the number of molecules entering a given functional pathway.

ACKNOWLEDGMENTS

R. Bolten and D. Egger contributed equally to this report.

This work was supported by grants 31-39175.93 and 7SUPJO 48538 from the Swiss National Science Foundation and grant 95-1365 from INTAS-RFBR.

We thank E. Wimmer, SUNY, Stony Brook, N.Y., for the plasmid pT7PV; E. Ehrenfeld, NIH, Bethesda, Md., for polyclonal PV anti-2C antiserum; C. Rahner and C. A. Levy for help with digital image processing; and V. Boyko for helpful comments on the RPA.

REFERENCES

1. **Aldabe, R., A. Barco, and L. Carrasco.** 1996. Membrane permeabilization by poliovirus proteins 2B and 2BC. J. Biol. Chem. **271:**23134–23137.
2. **Aldabe, R., and L. Carrasco.** 1995. Induction of membrane proliferation by poliovirus proteins 2C and 2BC. Biochem. Biophys. Res. Commun. **206:**64–76.
3. **Andino, R., G. E. Rieckhof, and D. Baltimore.** 1990. A functional ribonucleoprotein complex forms around the 5′ end of poliovirus RNA. Cell **63:**369–380.
4. **Banerjee, R., A. Echeverri, and A. Dasgupta.** 1997. Poliovirus-encoded 2C polypeptide specifically binds to the 3′-terminal sequences of viral negative-strand RNA. J. Virol. **71:**9570–9578.
5. **Baron, M. H., and D. Baltimore.** 1982. In vitro copying of viral positive strand RNA by poliovirus replicase. Characterization of the reaction and its products. J. Biol. Chem. **257:**12359–12366.
6. **Barton, D. J., E. P. Black, and J. B. Flanegan.** 1995. Complete replication of poliovirus in vitro: preinitiation RNA replication complexes require soluble cellular factors for the synthesis of VPg-linked RNA. J. Virol. **69:**5516–5527.
7. **Barton, D. J., and J. B. Flanegan.** 1997. Synchronous replication of poliovirus RNA: initiation of negative-strand RNA synthesis requires the guanidine-inhibited activity of protein 2C. J. Virol. **71:**8482–8489.
8. **Bienz, K., and D. Egger.** 1995. Immunocytochemistry and in situ hybridization in the electron microscope: combined application in the study of virus-infected cells. Histochem. Cell Biol. **103:**325–338.
9. **Bienz, K., D. Egger, and L. Pasamontes.** 1987. Association of polioviral proteins of the P2 genomic region with the viral replication complex and virus-induced membrane synthesis as visualized by electron microscopic immunocytochemistry and autoradiography. Virology **160:**220–226.
10. **Bienz, K., D. Egger, and T. Pfister.** 1994. Characteristics of the poliovirus replication complex. Arch. Virol. Suppl. **9:**147–157.
11. **Bienz, K., D. Egger, T. Pfister, and M. Troxler.** 1992. Structural and functional characterization of the poliovirus replication complex. J. Virol. **66:**2740–2747.

12. **Bienz, K., D. Egger, Y. Rasser, and W. Bossart.** 1980. Kinetics and location of poliovirus macromolecular synthesis in correlation to virus-induced cytopathology. Virology **100:**390–399.
13. **Bienz, K., D. Egger, Y. Rasser, and W. Bossart.** 1983. Intracellular distribution of poliovirus proteins and the induction of virus-specific cytoplasmic structures. Virology **131:**39–48.
14. **Bienz, K., D. Egger, M. Troxler, and L. Pasamontes.** 1990. Structural organization of poliovirus RNA replication is mediated by viral proteins of P2 genomic region. J. Virol. **64:**1156–1163.
15. **Caliguiri, L. A., and I. Tamm.** 1970. The role of cytoplasmic membranes in poliovirus biosynthesis. Virology **42:**100–111.
16. **Cao, X. M., R. J. Kuhn, and E. Wimmer.** 1993. Replication of poliovirus RNA containing two VPg coding sequences leads to a specific deletion event. J. Virol. **67:**5572–5578.
17. **Cho, M. W., N. Teterina, D. Egger, K. Bienz, and E. Ehrenfeld.** 1994. Membrane rearrangement and vesicle induction by recombinant poliovirus 2C and 2BC in human cells. Virology **202:**129–145.
18. **Cox, K. H., D. V. DeLeon, L. M. Angerer, and R. C. Angerer.** 1984. Detection of mRNAs in sea urchin embryos by in situ hybridization using asymmetric RNA probes. Dev. Biol. **101:**485–502.
19. **Dales, S., H. J. Eggers, I. Tamm, and G. E. Palade.** 1965. Electron microscopic study of the formation of poliovirus. Virology **26:**379–389.
20. **Egger, D., L. Pasamontes, R. Bolten, V. Boyko, and K. Bienz.** 1996. Reversible dissociation of the poliovirus replication complex: functions and interactions of its components in viral RNA synthesis. J. Virol. **70:**8675–8683.
21. **Etchison, D., and E. Ehrenfeld.** 1981. Comparison of replication complexes synthesizing poliovirus RNA. Virology **111:**33–46.
22. **Flanegan, J. B., and D. Baltimore.** 1979. Poliovirus polyuridylic acid polymerase and RNA replicase have the same viral polypeptide. J. Virol. **29:** 352–360.
23. **Girard, M.** 1969. In vitro synthesis of poliovirus ribonucleic acid: role of the replicative intermediate. J. Virol. **3:**376–384.
24. **Guinea, R., and L. Carrasco.** 1990. Phospholipid biosynthesis and poliovirus genome replication, two coupled phenomena. EMBO J. **9:**2011–2016.
25. **Harris, K. S., W. K. Xiang, L. Alexander, W. S. Lane, A. V. Paul, and E. Wimmer.** 1994. Interaction of poliovirus polypeptide $3CD^{pro}$ with the 5′ and 3′ termini of the poliovirus genome—identification of viral and cellular cofactors needed for efficient binding. J. Biol. Chem. **269:**27004–27014.
26. **Li, J. P., and D. Baltimore.** 1988. Isolation of poliovirus 2C mutants defective in viral RNA synthesis. J. Virol. **62:**4016–4021.
27. **Molla, A., A. V. Paul, and E. Wimmer.** 1991. Cell-free de novo synthesis of poliovirus. Science **254:**1647–1651.
28. **Molla, A., A. V. Paul, and E. Wimmer.** 1993. Effects of temperature and lipophilic agents on poliovirus formation and RNA synthesis in a cell-free system. J. Virol. **67:**5932–5938.
29. **Neufeld, K. L., J. M. Galarza, O. C. Richards, D. F. Summers, and E. Ehrenfeld.** 1994. Identification of terminal adenylyl transferase activity of the poliovirus polymerase $3D^{pol}$. J. Virol. **68:**5811–5818.
30. **Neufeld, K. L., O. C. Richards, and E. Ehrenfeld.** 1991. Purification, characterization, and comparison of poliovirus RNA polymerase from native and recombinant sources. J. Biol. Chem. **266:**24212–24219.
31. **Novak, J. E., and K. Kirkegaard.** 1991. Improved method for detecting poliovirus negative strands used to demonstrate specificity of positive-strand encapsidation and the ratio of positive to negative strands in infected cells. J. Virol. **65:**3384–3387.
32. **Novak, J. E., and K. Kirkegaard.** 1994. Coupling between genome translation and replication in an RNA virus. Genes Dev. **8:**1726–1737.
33. **Pasamontes, L., D. Egger, and K. Bienz.** 1986. Production of monoclonal and monospecific antibodies against non-capsid proteins of poliovirus. J. Gen. Virol. **67:**2415–2422.
34. **Paul, A. V., A. Molla, and E. Wimmer.** 1994. Studies of a putative amphipathic helix in the N-terminus of poliovirus protein 2C. Virology **199:**188–199.
35. **Paul, A. V., J. H. vanBoom, D. Filippov, and E. Wimmer.** 1998. Protein-primed RNA synthesis by purified poliovirus RNA polymerase. Nature **393:** 280–284.
36. **Restrepo-Hartwig, M. A., and P. Ahlquist.** 1996. Brome mosaic virus helicase- and polymerase-like proteins colocalize on the endoplasmic reticulum at sites of viral RNA synthesis. J. Virol. **70:**8908–8916.
37. **Sandoval, I. V., and L. Carrasco.** 1997. Poliovirus infection and expression of the poliovirus protein 2B provoke the disassembly of the Golgi complex, the organelle target for the antipoliovirus drug Ro-090179. J. Virol. **71:**4679–4693.
38. **Schaad, M. C., P. E. Jensen, and J. C. Carrington.** 1997. Formation of plant RNA virus replication complexes on membranes: role of an endoplasmic reticulum-targeted viral protein. EMBO J. **16:**4049–4059.
39. **Schlegel, A., T. H. Giddings, Jr., M. S. Ladinsky, and K. Kirkegaard.** 1996. Cellular origin and ultrastructure of membranes induced during poliovirus infection. J. Virol. **70:**6576–6588.
40. **Sitzmann, J. H., and P. K. LeMotte.** 1993. Rapid and efficient generation of PCR-derived riboprobe templates for in situ hybridization histochemistry. J. Histochem. Cytochem. **41:**773–776.
41. **Takegami, T., B. L. Semler, C. W. Anderson, and E. Wimmer.** 1983. Membrane fractions active in poliovirus RNA replication contain VPg precursor polypeptides. Virology **128:**33–47.
42. **Teterina, N. L., K. M. Kean, A. E. Gorbalenya, V. I. Agol, and M. Girard.** 1992. Analysis of the functional significance of amino acid residues in the putative NTP-binding pattern of the poliovirus 2C protein. J. Gen. Virol. **73:**1977–1986.
43. **Todd, S., J. S. Towner, D. M. Brown, and B. L. Semler.** 1997. Replication-competent picornaviruses with complete genomic RNA 3′ noncoding region deletions. J. Virol. **71:**8868–8874.
44. **Troxler, M., D. Egger, T. Pfister, and K. Bienz.** 1992. Intracellular localization of poliovirus RNA by in situ hybridization at the ultrastructural level using single-stranded riboprobes. Virology **191:**687–697.
45. **Van Dyke, T. A., and J. B. Flanegan.** 1980. Identification of poliovirus polypeptide P63 as a soluble RNA-dependent RNA polymerase. J. Virol. **35:**732–740.
46. **van Kuppeveld, F. J. M., J. M. Galama, J. Zoll, P. J. van den Hurk, and W. J. Melchers.** 1996. Coxsackie B3 virus protein 2B contains cationic amphipathic helix that is required for viral RNA replication. J. Virol. **70:**3876–3886.
47. **van Kuppeveld, F. J. M., J. M. D. Galama, J. Zoll, and W. J. G. Melchers.** 1995. Genetic analysis of a hydrophobic domain of coxsackie B3 virus protein 2B: a moderate degree of hydrophobicity is required for a *cis*-acting function in viral RNA synthesis. J. Virol. **69:**7782–7790.
48. **van Kuppeveld, F. J. M., P. J. van den Hurk, W. van der Vliet, J. M. Galama, and W. J. Melchers.** 1997. Chimeric coxsackie B3 virus genomes that express hybrid coxsackievirus-poliovirus 2B proteins: functional dissection of structural domains involved in RNA replication. J. Gen. Virol. **78:**1833–1840.
49. **Young, D. C., D. M. Tuschall, and J. B. Flanegan.** 1985. Poliovirus RNA-dependent RNA polymerase and host cell protein synthesize product RNA twice the size of poliovirion RNA in vitro. J. Virol. **54:**256–264.
50. **Young, I. D., R. J. Stewart, L. Ailles, A. Mackie, and J. Gore.** 1993. Synthesis of digoxigenin-labeled cRNA probes for nonisotopic in situ hybridization using reverse transcription polymerase chain reaction. Biotech. Histochem. **68:**153–158.